13.4 EXAMINATION OF ATMOSPHERIC WAVES ASSOCIATED WITH 13 MARCH 2003 BOW ECHO

Rebecca D. Adams-Selin[1]* and Richard H. Johnson[1]

[1]Department of Atmospheric Science,
Colorado State University, Fort Collins, Colorado

1. INTRODUCTION

The ability of linear convective systems to generate gravity waves is well-documented in the literature (Nicholls et al. 1987; Schmidt and Cotton 1990; Mapes 1993; Haertel et al. 2001, Fovell 2002, 2006; Knupp 2006; Parker 2008). It is also well known that these convective systems typically produce a pool of negatively buoyant air that propagates along the surface as a gravity or density current. Less well known is what surface patterns these feature produce, particularly in association with bow echoes.

Changes in heating and cooling rates in the atmosphere, as are often found with convection, can result in the generation of gravity waves (Nicholls et al. 1991; Fovell 2002, 2006). During the formation of a convective line a warming vertical temperature profile is typical, due to the latent heat release from condensation and freezing in the updraft. Previous studies (Gallus and Johnson 1991, Nicholls et al. 1991) have shown that this heating has an approximate first internal mode structure ($n = 1$) extending the entire depth of the troposphere. This heating profile incites a gravity wave that travels quickly away from its source. As is displayed in Fig. 1, a temporary low (high) pressure perturbation at the surface (aloft) is generated, along with an increase in the u wind flow toward the heating source at lower levels, and away from the heating source at upper levels (Nicholls et al. 1991). A dip in the potential temperature contours is also customary, generated by subsidence throughout the column. At the surface, this appears as a temporary dip in pressure unaccompanied by any change in temperature or wind. It was also noted by Mapes (1993) that the pre-storm environment is in some sense permanently modified by this wave. The subsidence causes slight warming and drying throughout the depth of the atmosphere, particularly in the mid-levels.

Additionally, the heating profile generated by a system's stratiform precipitation region, of $n = 2$ structure with cooling in low levels and heating aloft, can generate yet another low-frequency gravity wave. In this case, a high pressure perturbation is generated at the surface, with upward motion incited throughout the low levels. This wave moves more slowly than the $n = 1$ wave. Fovell et al. (2006) has noted that $n = 2$ wave energy can also modify the pre-storm environment. As the associated low-level updraft lifts the air, it is cooled and moistened. Frequently water condenses during this lifting, increasing the parcel's buoyancy, and small clouds are formed. This increase in buoyancy can act to locally strengthen the convective line as the newly formed clouds are overtaken by the main system, provided they have not already developed rainfall and their own associated cold pool.

A number of surface pressure features were evident in association with the 13 March 2003 bow echo studied by Adams-Selin and Johnson (2010, from now on ASJ10). Specifically, there was a fast-moving low pressure perturbation that formed in conjunction with the convective line and propagated quickly away. There was also a slower-moving high pressure perturbation that surged ahead of the convective line prior to new bowing development. The mesohigh surge prior to new bowing was noted in 35 of 39 bow echoes observed in Oklahoma over the 4-year ASJ10 study, suggesting a connection to bowing development. It was also suggested, although not confirmed, that both of these features could be explained by low-frequency gravity waves. However, only surface observations were available for that study, and thus the existence of gravity waves could not be stated with certainty. This study will use a high-resolution model simulation to determine if such features did exist, as well as examine resulting environmental effects. An idealized Cloud Model 1 simulation (CM1, Bryan and Fritsch 2002) was used to reproduce these pressure features and their cause.

A discussion of the 13 March 2003 bow echo and all observed pressure features will be given in Section 2. The two models used will be described in Section 3. Sections 4 and 5 will analyze the wave

*Corresponding author address: Rebecca Adams-Selin, 16th Weather Squadron, HQ AFWA, 101 Nelson Dr. Offutt AFB, NE 68113; rebecca.selin.ctr@offutt.af.mil

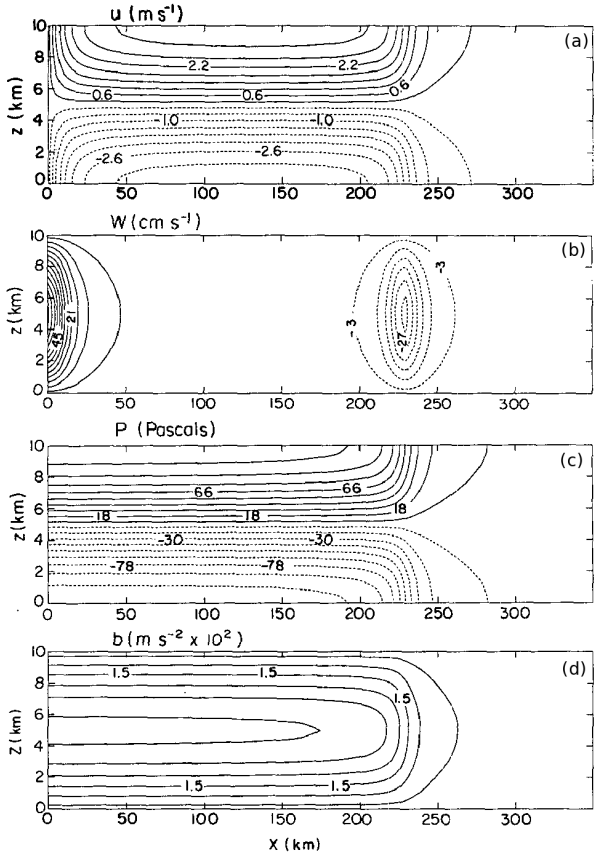

Figure 1: A rigid-lid gravity wave simulation for the n=1 vertical wave mode, from Nicholls et al. (1991). The depth of the 2.0 J kg^{-1} heating source extended through a 10 km "troposphere", with $N = 0.01$ s^{-1}. Shown is two hours into the simulation. (a) is u wind (0.4 m s^{-1}), (b) vertical velocity (6 cm s^{-1}), (c) perturbation pressure (0.12 hPa), and (d) perturbation buoyancy (0.006 m s^{-2}).

features simulated in the CM1 model. Finally, Section 6 states the conclusions.

2. 13 MARCH 2003 CASE REVIEW

2.1 *Fast-moving low pressure perturbation*

Figure 2, from ASJ10, displays composite WSI NOWrad radar reflectivity data, overlaid with high-pass Laczos-filtered pressure and temperature data from the Oklahoma Mesonet. (The high-pass filtering was designed to remove synoptic features from the data; see ASJ10 for more details.) The 13 March 2003 bow echo initialized as a convective line in central Oklahoma, in isolation from other convection at 0230 UTC (Fig. 2a). A low pressure region was evident centered over the convective line. This low pressure region quickly split and propagated away from the convective line (0345 UTC, Fig. 2b). A timeseries of data from Oklahoma Mesonet station VANO, shown by a black dot in Fig. 2, is given in Fig. 3. A dip in pressure, unaccompanied by a temperature change, is shown at arrow [a]. This would seem to be indicative of a gravity wave feature, as discussed above. This dip in pressure was tracked in numerous Mesonet stations across Oklahoma, and an average ground-relative speed of 34.1 m s^{-1} was calculated. The mean environmental tropospheric wind speed parallel to the direction of motion of the feature, 1.6 m s^{-1}, was computed using the 0000 UTC sounding from Norman, Oklahoma (KOUN, not shown). Accounting for this tailwind yields an actual feature speed of 32.5 m s^{-1}.

2.2 *Slower-moving high pressure surge*

The second pressure feature associated with the system was a mesohigh surge partially ahead of the convective line. Between 0345 and 0515 UTC (Figs. 2b, c) a mesohigh pressure perturbation formed over the convective line and spread southwestward as the convective intensity strengthened. At 0545 UTC (Fig. 2d) the mesohigh surged partially ahead of the convective line, and was shortly followed by new bowing development within the line at 0615 UTC (Fig. 2e). It was noted in ASJ10 that the size of the mesohigh pressure surge in this figure as produced by the objective analysis was too large. Based on an average system speed of 17.3 m s^{-1}, a time-space transformation of the interval between the initial pressure rise at station VANO (0535 UTC, [b] in Fig. 3) and the pressure peak (0555 UTC, [d]) yields a gradient width of 20.8 km. The width of the same pressure gradient in Fig. 2d, however, is approximately 60 km. Thus, it should be noted that while the mesohigh surge ahead of the convective line exists, its size is overestimated by about a factor of three. Multiple objective analysis methods were tried in an attempt to fix this overestimation, but it was an inherent problem in all analysis methods.

A re-examination of Fig. 3 shows a sharp increase in pressure, a wind shift of almost 180 degrees, and an increase in wind speed all at 0535 UTC (arrows [b], [c]), but no accompanying potential temperature drop. The sharp temperature drop and onset of rain at 0555 UTC (arrows [d] and [e]) indicated the arrival of the surface cold pool or gravity current. This pressure rise, significantly in advance of the temperature drop, occurred at almost all Mesonet stations passed by the bow echo system. These observations could be indicative of one of three features: a low-frequency gravity wave gen-

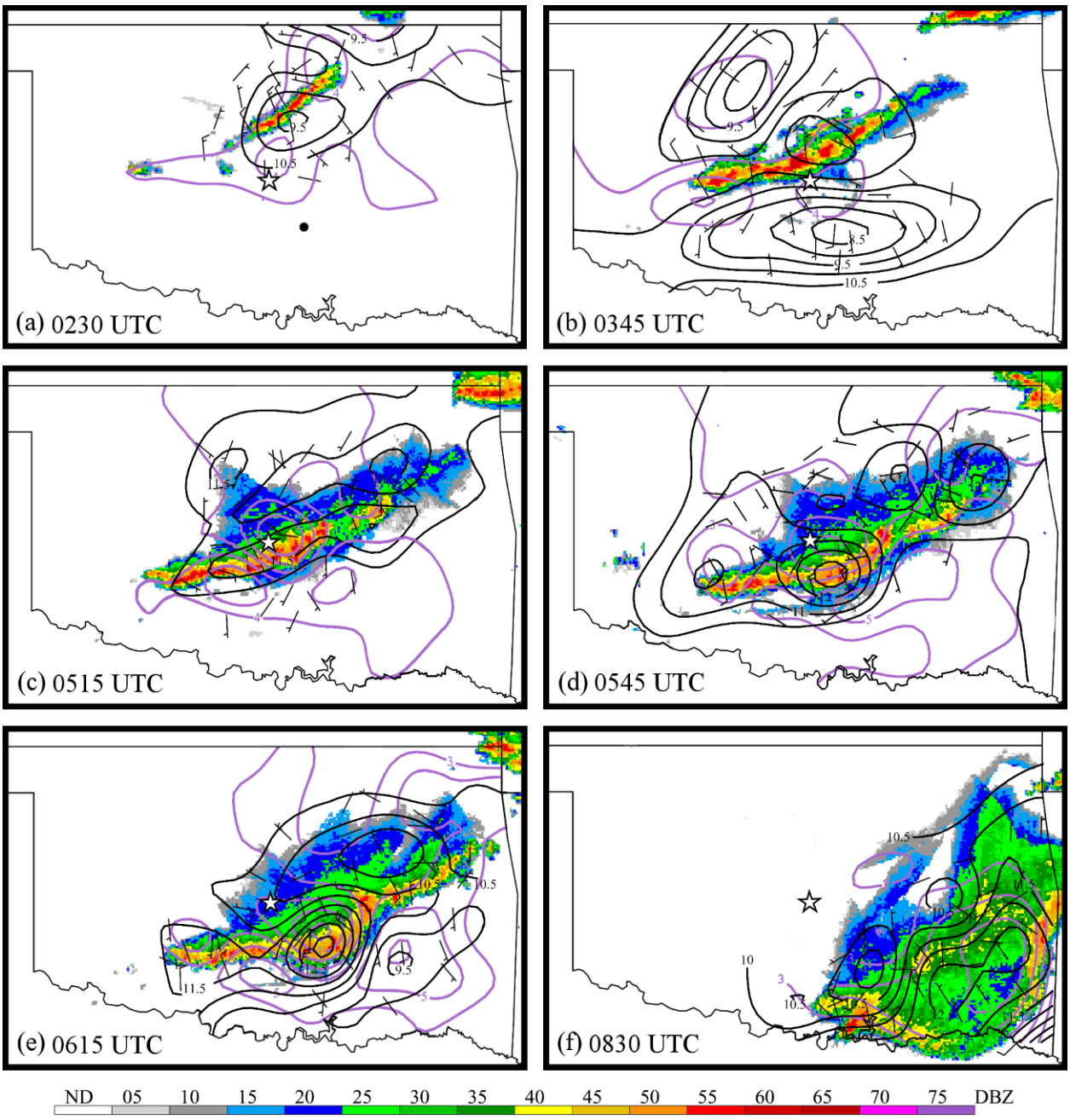

Figure 2: WSI NOWrad base reflectivity from 0230 (a), 0345 (b), 0515 (c), 0545 (d), 0615 (e), and 0830 (f) UTC 13 March 2003. High-pass filtered potential temperature (purple, 1°C), surface wind (black, barbs) and adjusted pressure (black, 0.5 hPa). The star is the KTLX radar, and the black dot in (a) is mesonet station VANO. (From ASJ10.)

erated by low-level cooling behind the convective line; a non-hydrostatic pressure response to an intensifying cold pool; or a bore propagating ahead of the system in a stable boundary layer. Unfortunately, without observations above the surface, analyzing this feature requires numerical modeling.

3. MODEL DESCRIPTION

CM1 was initialized with the 0000 UTC 13 March 2003 Norman, Oklahoma (KOUN) sounding, which is shown in Fig. 4. Other than minor smoothing to remove instabilities and extrapolation of missing moisture data at upper levels, the sounding was unmodified. The domain covered 600 km (x direction) by 400 km (y direction) by 18 km vertically. A horizontal resolution of 1 km was used, with a constant vertical resolution of 250 m, and a 3 s time step. Other than the Thompson et al. (2008) microphysics parameterization, no other parameterizations were used. As the observed bow echo occurred at night, a time of minimal boundary layer mixing, the lack of a boundary layer parameterization was considered acceptable for an initial approach. Future work will include radiational cooling along with a boundary layer parameterization, to allow a nighttime stable layer to develop. The "cold pool-dam break" convective initialization method was used. In this method, a "cold dam" of air was created along the left side of the domain by decreasing the initial potential temperature. This was done from 0 to 200 km in the x-direction, and 50 to 350 km in the y-direction. The magnitude of the potential temperature decrease was 6 K at that surface, and linearly decreased until reaching 0 K 2.5 km aloft. As the simulation began, the cold pool dam would "break" and surge forward as a gravity current. Air in advance of the gravity current would be forced upward, eventually generating convection.

4. FIRST LOW-FREQUENCY GRAVITY WAVE

Within the CM1 simulation, convection first initializes at 0:15 simulation time, directly over the edge of the gravity current. By 0:35 the convection reaches above 12 km vertically, and remains there for the rest of the simulation. Also at this time, a low pressure perturbation of -1 hPa is evident parallel to and just ahead of the convective line (not shown). At 1:00 (Fig. 5a) the low pressure region has moved quickly ahead of the convective line; it continues propagating toward the right side of the domain (Fig. 5b) while decreasing in magnitude, until it leaves the domain area at 03:30 (not shown). This compares well to the observed fast-moving low pressure regions that propagated away from the convective system.

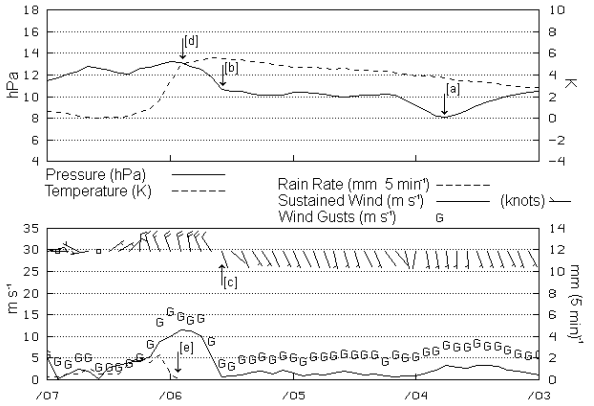

Figure 3: Timeseries display of high-pass filtered data for station VANO of the Oklahoma Mesonet, as shown by the black dot in Fig. 2, which experienced both the pressure surge and the newly bowed segment of the bow echo. Time increases to the left, from 0300 to 0700 UTC on 13 Mar 2003. Upper graph shows potential temperature (K, dashed, upper right scale) and adjusted pressure (hPa, solid line, upper left scale). Lower graph shows sustained winds (knots, barbs), sustained wind speed (m s^{-1}, solid line, lower left scale), unfiltered wind gusts (m s^{-1}, "G", lower left scale), and unfiltered precipitation rate (mm (5 min)$^{-1}$, dashed line, lower right scale). [a] is the dip in pressure signifying the passage of the fast–moving low pressure feature (0345 UTC). [b] and [c] are the start of the sharp pressure rise and the wind shift (0535 UTC). [d] is the sharp potential temperature drop (0555 UTC) and arrival of the cold pool. [e] is the start of precipitation, at the same time. From ASJ10.

Vertical cross-sections during this time period show strong similarities to the perturbations typically produced by a gravity wave generated by the first internal mode of deep heating (Fig. 1). A high pressure perturbation is evident aloft, over a low pressure perturbation at the surface (Fig. 6a). The low pressure perturbation corresponds to that seen in the plan view in Fig. 5. A dip in the potential temperature contours is collocated with the pressure perturbations; this dip could be due to the subsidence warming associated with the downdraft at the leading edge of a gravity wave. The u wind perturbation field also agrees well with the theoretical results from Nicholls et al. (1991). The environmental flow towards the system is strengthened from the surface to 6 km aloft, with the most intense strengthening between 2 to 3 km. The flow away from the system was also intensified, at 6 km and above, with the most intense areas at 6.5 km and 9 km.

Soundings from before and after gravity wave passage show a small amount of warming and drying

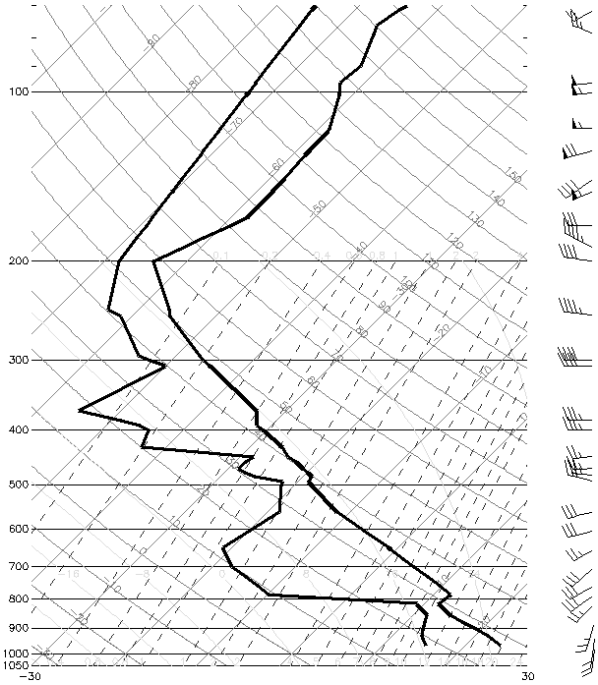

Figure 4: KOUN 0000 UTC 13 March 2003 sounding, as modified for use in the CM1 simulation.

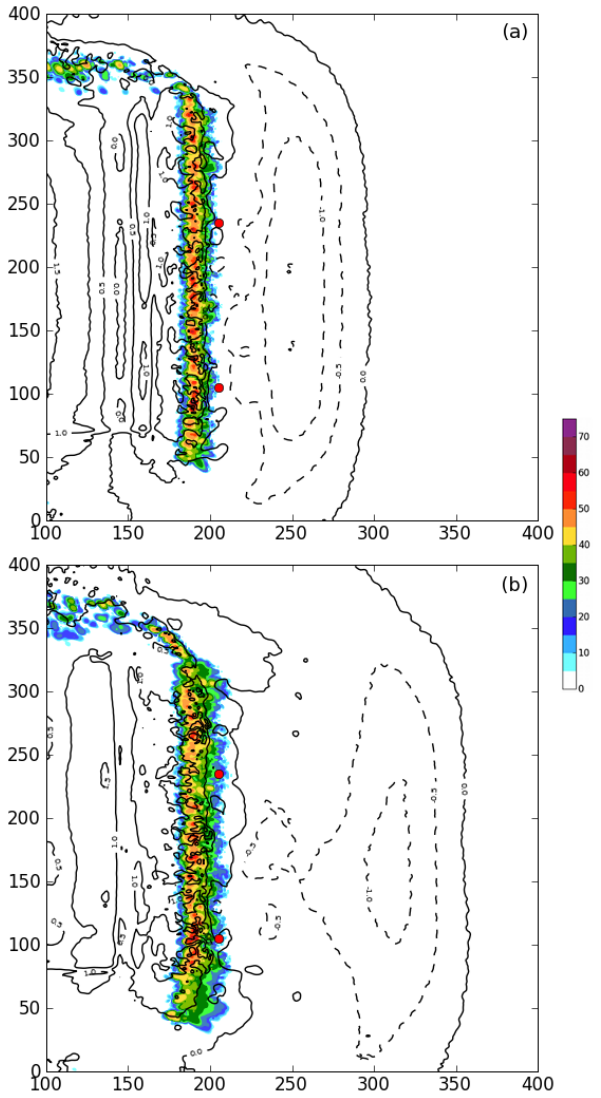

Figure 5: Composite reflectivity from the CM1 simulation. Only a portion of the domain is shown for space considerations. From 1:00 (a), 1:30 (b) after simulation start. Perturbation pressure (0.5 hPa, dashed negative) in black. Convection in the upper left portion of the domain is due to the "cold-dam" box initiation method.

that occurs over the mid-levels of the atmosphere (Fig. 7). This correlates strongly with the results of Mapes (1993) that the low-frequency gravity waves generated by convective heating do not act entirely like waves, which would return the atmosphere to its pre-passage state. Instead, a small amount of warming and drying should occur throughout the depth of the atmosphere, particularly in the mid-levels. The model soundings before and after wave passage also show the winds were modified by the passage of the wave, with a slowing of the westerly flow in the lower levels, and an increase in westerly flow aloft (Fig. 7) as was also shown in the u wind perturbation fields in the previous figure. Essentially this was an intensification of storm-relative inflow at lower levels, and of outflow aloft. Thus, while the wave negatively affects the pre-storm environment by slightly warming and drying the mid-levels ahead of the storm, it also favorably alters the wind profile to improve the storm-relative flow.

The gravity wave speed was calculated assuming wave motion in the x direction only. Taking into account the mean tropospheric wind speed in direction of wave motion (18.1 m s^{-1}) and the 15 m s^{-1} translation of the domain in the in x-direction, the total gravity wave speed is 29.9 m s^{-1}. This is very close to the observed wave speed in the 13 March 2003 case of 32.5 m s^{-1} (ASJ10), especially considering the idealized simulation contained no synoptic influences on the stability of the atmosphere.

5. SECOND GRAVITY WAVE

At 1:15 simulation time, the perturbation pressure contours appeared approximately parallel to the convective line and associated cold pool, as would be expected from hydrostatic theory (Fig. 8a). However, at 1:55, two positive pressure perturbations could be seen surging approximately 10 km ahead of the convective line (Fig. 8b). The bottom two red dots in Fig. 8 correspond to the two pressure surges, and the top dot to a location in the line with

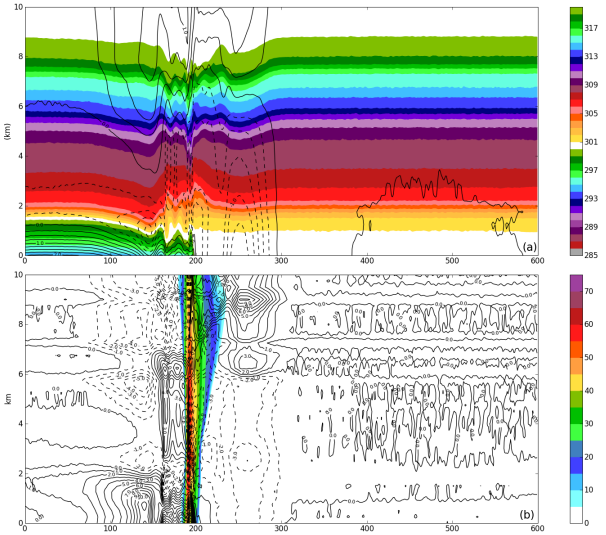

Figure 6: CM1 vertical cross-sections at 1:00 simulation time, averaged about 5 gridpoints either side of a y=110 km line. (a) Total potential temperature (K, color), with pressure perturbation (black, 0.25 hPa, negative dashed). (b) Simulated reflectivity (dbZ, color), u wind perturbation (black, 1 m s^{-1}, negative dashed).

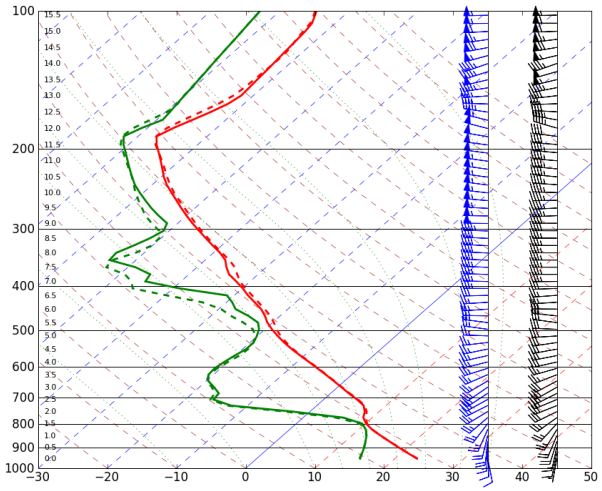

Figure 7: Soundings from CM1 simulation from before (1:25; solid temperature and dewpoint trace; black winds) and after (2:25; dashed temperature and dewpoint trace; blue winds) gravity wave passage. Heights (km) are plotted along the pressure axis. An average of all model gridpoints within x=350 and y=102 to 108.

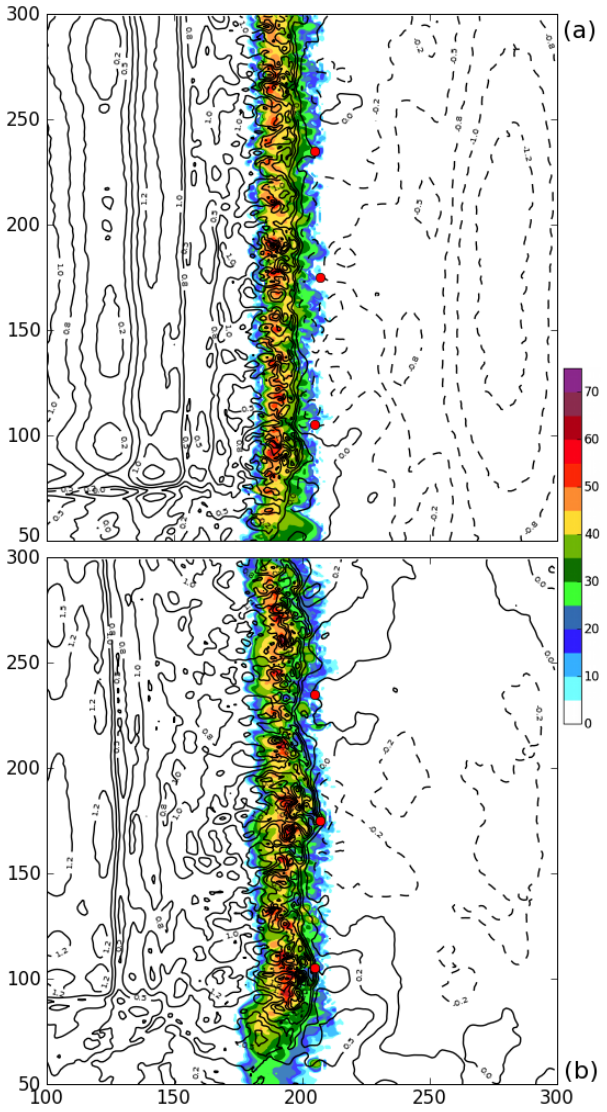

Figure 8: Simulated composite reflectivity from the CM1 idealized simulation. From 1:15 (a), 1:55 (b) after simulation start. Perturbation pressure (0.2 hPa) in black with negative perturbation dashed. The two bottommost red dots show the location of the two mesohigh pressure surges; the top dot indicates a portion of the convective line with no pressure surge. (Middle surge becomes larger after 20 min.)

no surge. A timeseries from the "southern" surge (Fig. 9a) shows a pressure rise occurring approximately 20 min prior to the arrival of the cold pool. The wind speeds at the time of the pressure surge did not change (not shown), further indicating that the gravity current has not yet arrived as gravity currents typically are characterized by rear-to-front flow at the surface. After 2:00, there are numerous oscillations in the pressure field, with an overall "permanent" rise in the pressure field. The timeseries from the "no surge" point (Fig. 9b) shows the pressure rise and temperature drop to be almost simultaneous (offset by 5 min). This is more reflective of a simple pressure response to a passing gravity current.

Plots of the temperature and dewpoint 2.5 km aloft of the same "surge" and "no surge" points are shown in Fig. 10. In the "surge" timeseries (Fig. 10a), the large fluctuations in temperature and dewpoint fit well with the idea of a gravity wave propagating through the lower-levels ahead of the

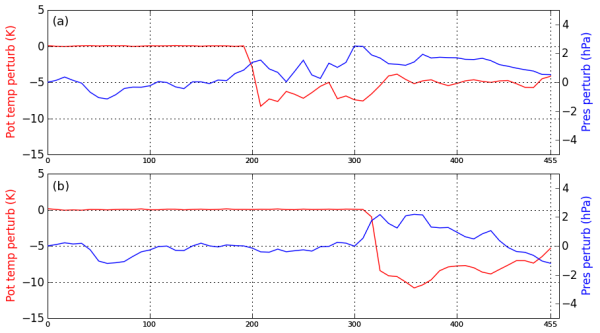

Figure 9: Surface timeseries from the CM1 simulation. Time increases to the right, with 100 = 1 h; 200 = 2 h, etc. From points (shown in Fig. 8) that (a) experience a pressure surge and (b) experience no surge. Red line is potential temperature perturbation (left axis, K); blue line is pressure perturbation (right axis, hPa).

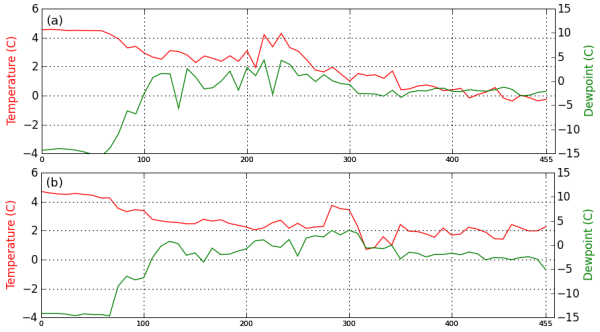

Figure 10: Timeseries from CM1 simulation at 2.5 km aloft. Time increases to the right, with 100 = 1 h; 200 = 2 h, etc. Top plot (a) is from the bottom point in Fig. 8, with the mesohigh surge; bottom plot (b) from the top point with no surge. Red line is temperature (^{o}C); green line dewpoint (^{o}C).

system at approximately 2.5 km. These fluctuations first appear over an hour prior to the gravity current passage, also indicative of a gravity wave feature. There is also an overall moistening and slight cooling of the level as wave oscillations begin passing after 1:00. Fovell et al. (2006) noted a similar development of a low-level "moist tongue" created by a gravity wave generated by the n=2 mode of heating. While a cooling and moistening of the layer is also evident in the "no surge" timeseries as the convective line approaches (Fig. 10b), the oscillations are minimal.

Cross-sections of the system through the southern pressure surge, both before the pressure surge formed (1:20 simulation time, Fig. 11), and during the time of the pressure surge (1:45 and 1:55, Figs. 12 and 13 respectively) are shown. At 1:20, the pressure response in advance of the system is minimal, and the low-level downdraft is comparatively weak (Fig. 11b, c). At 1:45, the low-level downdraft between 0.5 and 2.5 km strengthens (Fig. 12c). At this point it is unclear what causes this increase. The low-level downdraft extends through too deep a vertical layer for it to be due to a "rotor" formed at the head of the gravity current. There is also no increase in the intensity of rear inflow into the system at mid-levels, but it does now strengthen and extend vertically to the surface (Fig. 12d).

The stronger downdraft impinges on the cold pool, causing a dip in the potential temperature contours immediately behind the gravity current head (Fig. 12a). Storm-relative surface winds also increase (Fig. 12d). Ten minutes later, at 1:55 (Fig. 13a), a "recovery" in the cold pool is evident as its height increases. The surface outflow within the gravity current continues to increase as well (Fig. 13d). A strong positive pressure perturbation is evident propagating ahead of the system in response to the cold pool height increase (Fig. 13b). Small updraft-downdraft couplets, approximately 2.5 km aloft, correspond to oscillations within this pressure response (Fig. 13c). Within the updrafts, small clouds are formed due to condensation forced by the lifting of the air (Figs. 12b, 13b).

These results are very similar to those found in simulations by Fovell et al. (2006) where clouds and even rain were generated discretely in advance of the convective system by gravity waves. No rainwater or cold pools were associated with these small clouds. As in Fovell et al. (2006), these clouds are incorporated into the main updraft, and hence the convective line should locally intensify due to the small increase in positive buoyancy. This process could act as a positive feedback mechanism, strengthening the main low-level convective updraft-downdraft couplet, and then generating another gravity wave. Multiple cycles of this process are noted in the CM1 simulation (not shown), although only one iteration was strong enough to result in a surface mesohigh surge. The local intensification of the convective line could also assist in new bowing development.

6. CONCLUSIONS

The goal of this study was to examine the surface pressure features observed with the 13 March 2003 bow echo by Adams-Selin and Johnson 2010, determine if they could be associated with gravity waves, and if so examine how these features might modify the surrounding environment. There were two pressure features in question. The first was a region of low pressure, generated shortly after convective initialization, that spread quickly away from the convective line. The second was a surge of the mesohigh pressure region partially ahead of the con-

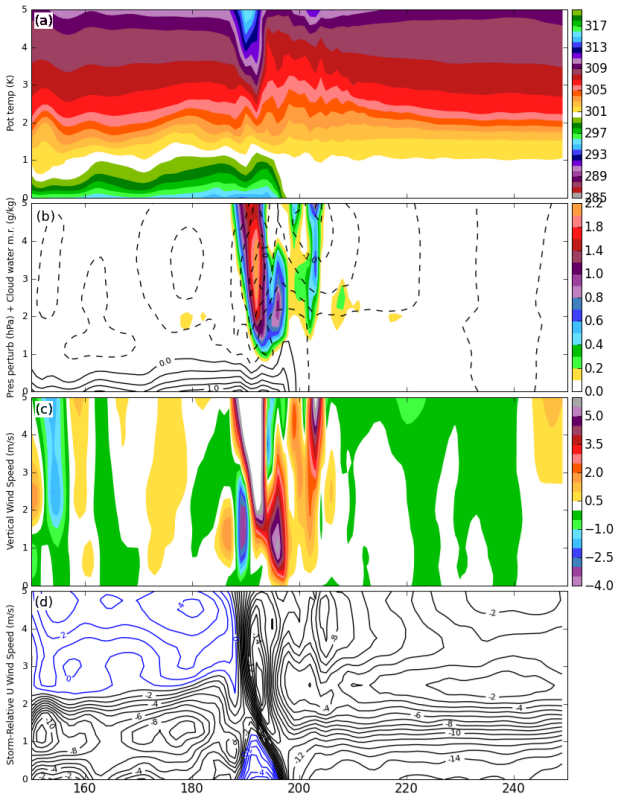

Figure 11: Four-panel cross-section from 1:20 CM1 simulation time. (a) is total potential temperature (color, 1K); (b) perturbation pressure (0.25 hPa, black lines, negative dashed) and cloud water mixing ratio (color, 0.1 g kg^{-1}); (c) vertical wind speed (color, 0.5 m s^{-1}); (d) storm-relative u wind speed (1 m s^{-1}, blue positive, black negative). X axis is km.

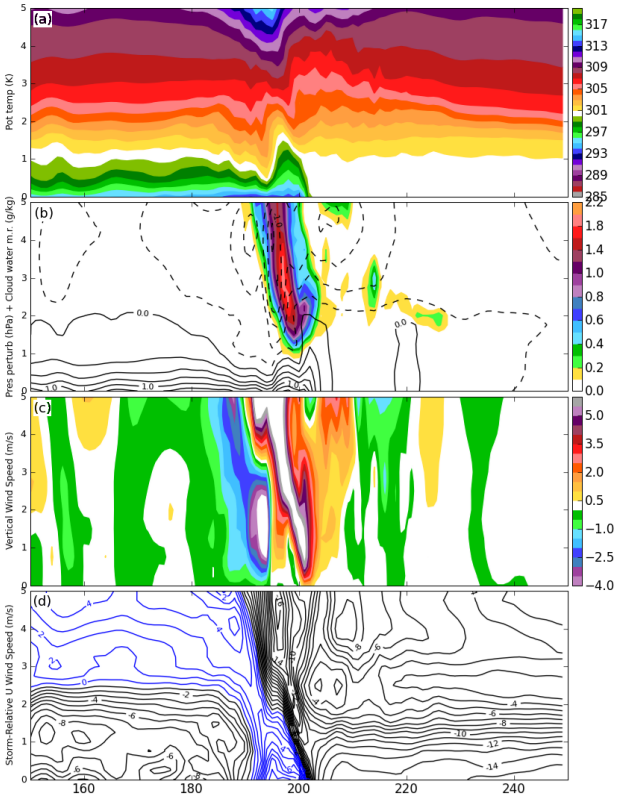

Figure 12: As in Fig. 11, but for 1:45 CM1 simulation time.

vective line immediately prior to new bowing development. The mesohigh surge was observed with a number of other bow echo systems also examined by ASJ10, hinting at importance. An idealized simulation using the CM1 model was used in an attempt to simulate these pressure features and determine their cause.

Within the CM1 simulation, the surface low pressure perturbation region that moved swiftly away from the convective line was determined to be a reflection of a $n = 1$ mode gravity wave, likely generated by the deep heating within the initializing convective line. The wave produced a low pressure perturbation at the surface, overtopped by a high pressure perturbation aloft; storm-relative inflow (outflow) was enhanced at lower (upper) levels. These features match those generated by the theoretical $n = 1$ gravity wave produced in Nicholls et al. (1991). The speed of the simulated wave was 29.9 m s^{-1}, very close to the observed speed of the low pressure feature, 32.5 m s^{-1}. This is particularly close when it is considered that the idealized simulation contained no synoptic influence on environmental stability.

The mesohigh pressure surge was generated by a second gravity wave within the CM1 simulation. Cross-sections through the convective line at that point revealed updraft-downdraft couplets associated with pressure oscillations, as well as small clouds that formed within each updraft, all embedded within the broader-scale surge feature. The discussed evidence is suggestive of the mechanisms proposed by Fovell et al. (2006). In that study, the low levels ahead of the convective line are cooled by a low-frequency gravity wave, generated in response to the $n = 2$ heating profile of the associated stratiform precipitation region. In addition, isolated clouds develop on top of this layer in response to high-frequency gravity waves generated by short-term fluctuations in the heating or cooling rates of the convective line. These waves are ducted ahead of the system by a leading anvil aloft. The extent to which these mechanisms apply to our case is not obvious as there was minimal trailing stratiform precipitation, as well as only a minimal anvil. These was, however, a strong trapping level as determined from the Scorer parameter at approximately 3 km; this could have acted to duct the high-frequency

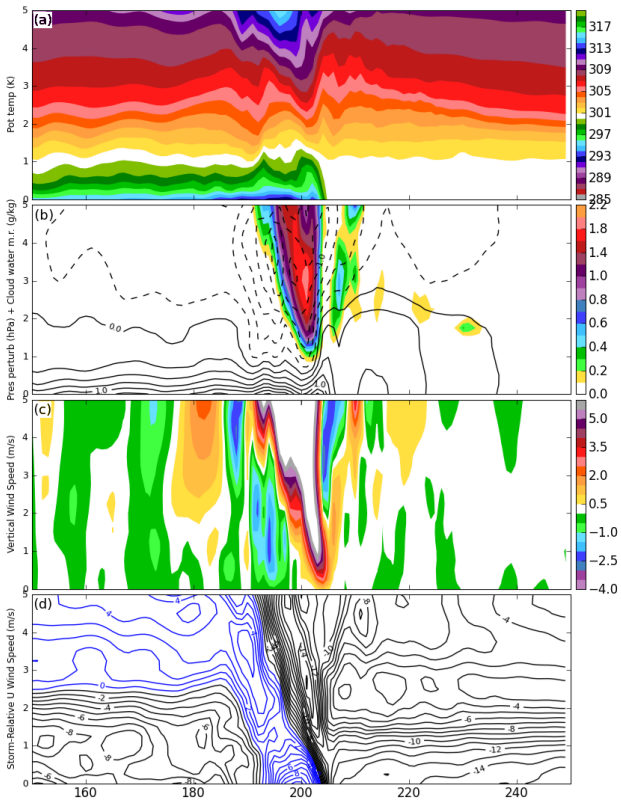

Figure 13: As in Fig. 11, but for 1:55 CM1 simulation time.

gravity waves. There is also the possibility that the strong downdraft that developed at 1:45 could have excited an $n = 3$ mode gravity wave, which would have moved ahead of the convective line producing ascent and cooling at low levels, as has been described by Lane and Reeder (2001) and Lane and Zhang (2011). Further study is needed to sort out the processes relevant to this case.

Furthermore, the methods of generation of the fast-moving gravity waves within the CM1 simulation have not been fully examined. Current theory (Nicholls et al. 1991, Haertel et al. 2001) suggests that the first, fast-moving gravity wave should be generated by deep convective heating. The second gravity wave, depending on its frequency, should be produced by either long- or short-term changes in the rate of low-level cooling. Future work will include examining simulated heating and cooling rates, particularly those generated by microphysical processes, that could be acting to generate the waves. Simulations with radiational cooling will also be performed, to determine the effects of increasing environmental stability on wave generation. It is also expected the transition of a linear convective system from a surface-based, gravity current structure to an elevated, gravity wave structure would affect generation of the wave features.

7. ACKNOWLEDGMENTS

This research was supported by National Science Foundation Grant ATM-0500061. Computing resources were provided by the Navy Department of Defense Supercomputing Resource Center (Navy DSRC) and the Army Research Laboratory Department of Defense Supercomputing Resource Center (ARL DSRC), which are sponsored by the DoD High Performance Computing Modernization Program. Oklahoma Mesonet data were provided through the courtesy of the Oklahoma Mesonet, a cooperative venture between Oklahoma State University and the University of Oklahoma and supported by the taxpayers of Oklahoma. The WSI NOWrad data were provided by the Mesoscale and Microscale Meteorology Division of the University Corporation for Atmospheric Research (UCAR) through David Ahijevych. The authors would like to thank Drs. Susan van den Heever of CSU, and Morris Weisman and George Bryan of NCAR, for discussions regarding this work and assistance in using the CM1 models.

8. REFERENCES

Adams-Selin, R. D. and R. H. Johnson, 2010: Mesoscale surface pressure and temperature features associated with bow echoes. *Mon. Wea. Rev.*, **138**, 212–227.

Bryan, G. H. and J. M. Fritsch, 2002: A benchmark simulation for moist nonhydrostatic numerical models. *Mon. Wea. Rev.*, **130**, 2917–2928.

Fovell, R. G. 2006, G. L. Mullendore, and S.H. Kim, 2006: Discrete propagation in numerically simulated nocturnal squall lines. *Mon. Wea. Rev.*, **134**, 3735–3752.

——, R. G. 2002: Upstream influence of numerically simulated squall-line storms. *Quart. J. Roy. Meteorol. Soc.*, **128**, 893–912.

Gallus, W. A. Jr. and R. H. Johnson, 1991: Heat and moisture budgets of an intense midlatitude squall line. *J. Atmos. Sci.*, **48**, 122-146.

Haertel, P. T. R. H. Johnson, and S. N. Tulich, 2001: Some simple simulations of thunderstorm outflows. *J. Atmos. Sci.*, **58**, 504–516.

Knupp, K. 2006: Observational analysis of a gust front to bore to solitary wave transition within an evolving nocturnal boundary layer. *J. Atmos. Sci.*, **63**, 2016–2035.

Lane, T. P. and F. Zhang, 2011: Coupling between gravity waves and tropcial convection at mesoscales. *J. Atmos. Sci.*, *in press.*

——, T. P. 2001: Convectively generated gravity waves and their effect on the cloud environment. *J. Atmos. Sci.*, **58**, 2427–2440.

Mapes, G. E. 1993: Gregarious tropical convection. *J. Atmos. Sci.*, **50**, 2026–2037.

Nicholls, M. E. R. A. Pielka, and W. R. Cotton, 1991: Thermally forced gravity waves in an atmosphere at rest. *J. Atmos. Sci.*, **48**, 1869–1884.

Schmidt, J. M. and W. R. Cotton, 1990: Interactions between upper and lower tropospheric gravity waves on squall line structure and maintenance. *J. Atmos. Sci.*, **47**, 1205-1222.

Thompson, G. P. R. Field, R. M. Rasmussen, and W. D. Hall, 2008: Explicit forecasts of winter precipitation using an improved bulk microphysics scheme. Part II: Implementation of a new snow parameterization. *Mon. Wea. Rev.*, **136**, 5095–5115.